minerals

MDPI

Article

Geochemical, Isotopic and Petrological Constraints on the Origin and Evolution of the Recent Silicic Magmatism of the Greater Caucasus

Vasily Shcherbakov [1,2,*], Ilya Bindeman [1,3] and Viktor Gazeev [4]

1 Fersman Mineralogical Museum of the Russian Academy of Sciences, 119071 Moscow, Russia; bindeman@uoregon.edu
2 Geological Department, Lomonosov Moscow State University, 119234 Moscow, Russia
3 Department of Earth Sciences, University of Oregon, Eugene, OR 97403, USA
4 Institute of Geology of Ore Deposits, Petrography, Mineralogy and Geochemistry (IGEM) of the Russian Academy of Sciences, 119017 Moscow, Russia; vik.gaz.54@mail.ru
* Correspondence: vsh@geol.msu.ru

Abstract: Significant volumes of rhyolites and granites of the Pliocene-Pleistocene age are exposed in the collision zone of the Greater Caucasus, Russia. The volcanic history of the region includes ignimbrites and lavas associated with the Chegem caldera (2.9 Ma) and Elbrus volcano (1.98 and 0.7 Ma) and rhyolitic necks and granites in Tyrnyauz (1.98 Ma). They are characterized by a similar bulk and mineral composition and close ratios of incompatible elements, which indicates their related origin. The 1.98 Ma Elbrus ignimbrites, compared to the 2.9 Ma Chegem ignimbrites, have elevated concentrations of both compatible (Cr, Sr, Ca, Ni) and incompatible elements (Cs, Rb, U). We argue that the Elbrus ignimbrites were produced from magma geochemically similar to Chegem rhyolites through fractionation crystallization coupled with the assimilation of crustal material. The 1.98 Ma Eldjuta granites of Tyrnyauz and early ignimbrites of the Elbrus region (1.98 Ma) are temporally coeval, similar mineralogically, and have comparable major and trace element composition, which indicates that the Elbrus ignimbrites probably erupted from the area of modern Tyrnyauz; the Eldjurta granite could represent a plutonic reservoir that fed this eruption. Late ignimbrites of Elbrus (0.7 Ma) and subsequent lavas demonstrate progressively more mafic mineral assemblage and bulk rock composition in comparison with rhyolites. This indicates their origin in response to the mixing of rhyolites with magmas of a more basic composition at the late stage of magma system development. The composition of these basic magmas may be close to the basaltic trachyandesite, the flows exposed along the periphery of the Elbrus volcano. All studied young volcanic rocks of the Greater Caucasus are characterized by depletion in HSFE and enrichment in LILE, Li, and Pb, which emphasizes the close relationship of young silicic magmatism with magmas of suprasubduction geochemical affinity. An important geochemical feature is the enrichment of U up to 8 ppm and Th up to 35 ppm. The trace element composition of the rocks indicates that the original rhyolitic magma of Chegem ignimbrites caldera was formed at >80%–90% fractionation of calc-alkaline arc basalts with increased alkalinity. This observation, in addition to published data for isotopic composition (O-Hf-Sr) of the same units, shows that the crustal isotopic signatures of silicic volcanics may arise due to the subduction-induced fertilization of peridotites producing parental basaltic magmas before a delamination episode reactivated the melting of the former mantle and the lower crust.

Keywords: rhyolite; ignimbrite; Elbrus; Chegem caldera; collisional magmatism

check for updates

Citation: Shcherbakov, V.; Bindeman, I.; Gazeev, V. Geochemical, Isotopic and Petrological Constraints on the Origin and Evolution of the Recent Silicic Magmatism of the Greater Caucasus. *Minerals* **2022**, *12*, 105. https://doi.org/10.3390/min12010105

Academic Editors: Sung Won Kim and Dominique Gasquet

Received: 13 October 2021
Accepted: 12 January 2022
Published: 16 January 2022

1. Introduction

The widespread occurrence of silicic magmatism (granite intrusions, batholiths, and rhyolites) is typical for collisional environments, and their origin is debated. The source of silicic magmas can be the anatexis of crustal material, the differentiation of mantle-derived mafic magmas, or commonly a combination of these two mechanisms [1,2]. The source, age, geochemical characteristics, and temporal evolution of silicic magmatism of collision zones and elsewhere are critical for geodynamic reconstructions. The primary sources of information the origin of silicic magmas are the isotopic composition, mineralogical and geochemical features. For example, the Himalayan leucogranites are considered a result of the anatexis of radioactively heated thickened crust [3]. These units inherit purely crustal highly radiogenic isotopic ratios, are characterized by high $\delta^{18}O$ values (>10‰), and are enriched in incompatible elements. Silicic magmas formed by the fractionation of mantle-derived magmas have lower concentrations of incompatible trace elements, lower $\delta^{18}O$ values (6–8‰), and mantle-like radiogenic isotopic ratios [4–6].

This work characterizes petrological, mineralogical, and geochemical features of Pliocene-Holocene silicic lavas, tuffs and ignimbrites of Chegem and Elbrus, and Eldjurta granite of the Greater Caucasus, Russia, to provide petrological insight into their source and mutual genetic relationships.

2. Geological Relations and Magmatism Ages

Young syn-collisional volcanic and plutonic silicic rocks of Chegem, Tyrnyauz, and Elbrus areas are exposed in the collision zone of the Greater Caucasus (Figure 1). The 1.98 Ma Eldjurta granite massif in the Tyrnyauz area is one of the youngest granites exposed in a collisional environment worldwide, and is located 35 km northeast of Elbrus. Tyrnyauz is well-known for its industrially mined Mo-W deposits [7,8]. Eldjurta granite is intruded into Proterozoic-Paleozoic schists and gneisses and Paleozoic volcaniclastic formations. Chegem caldera (~11 × 15 km, 2.9 Ma) is 10 km southeast of Tyrnyauz. Its famously exposed 2 km-thick densely welded intracaldera rhyolitic tuff (ignimbrite), less welded voluminous outflow tuff sheets to the north (near Zayukovo village; Figure 1), and granodiorites are well exposed and were recently interpreted as being a result of a single large caldera-forming eruption by [9,10], while previous researchers advocated for several eruptions and multiple vents [11]. Chegem granodiorites are inside the uplifted intracaldera welded tuff, and the caldera is hosted by Palaeozoic gneisses and granites of Greater Caucasus crystalline core and sedimentary rock.

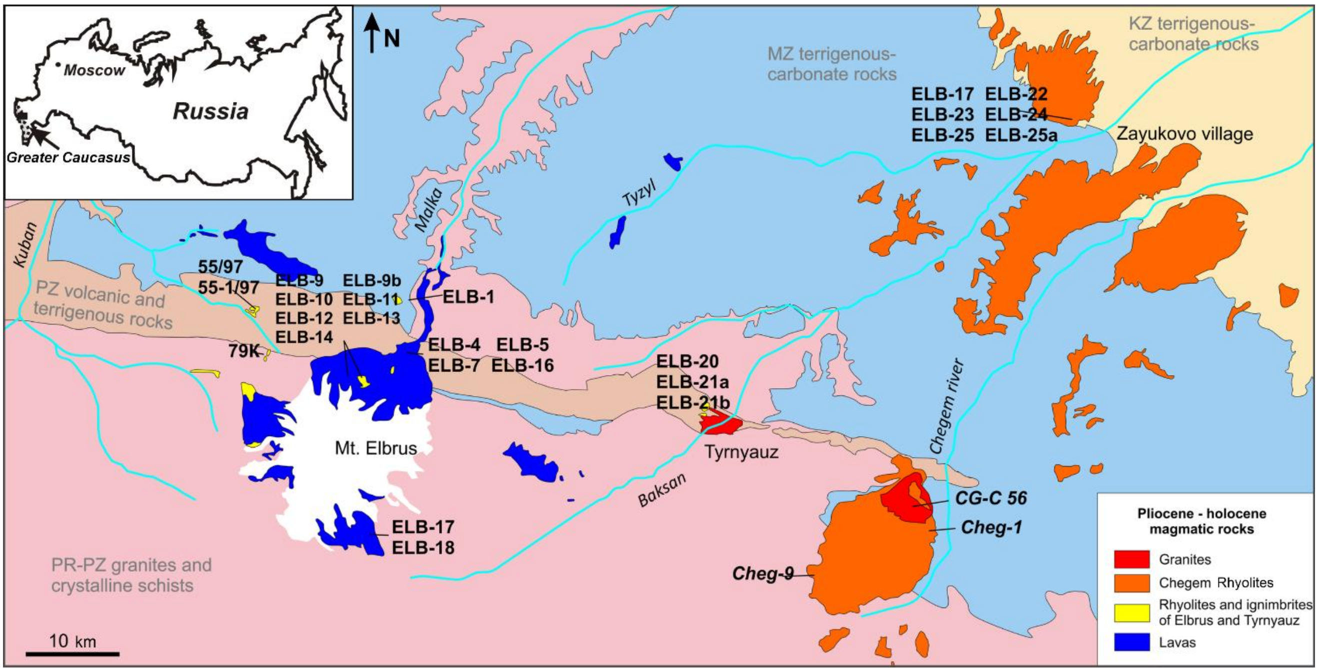

Figure 1. General geological structure and the Neogene-Quaternary volcanic and plutonic rocks of the Chegem and Elbrus area. The inset illustrates the Greater Caucasus location.

Tyrnyauz-area rhyolites are represented by rhyolitic volcanic necks on top of Eldjurta granite [12] and poorly dated rhyolitic fields to the west and north (Figure 1). Glacially eroded outcrops of rhyolitic tuffs are distributed mainly to the north and west parts of the modern volcanic edifice of Elbrus [13] (Figure 1) and likely extend to the basement of Elbrus edifice. Near Kukurtli ignimbrites form 1 km-thick wall with spectacular vertical welding features [13]. The high erosion rate of the rapidly uplifting Greater Caucasus led to the dissection of ignimbrite outcrops, which complicates the determination of geological relationships, the cross-correlation of individual sections, and the estimation of overall volumes of magmatism. Rhyolitic ignimbrites of different ages are exposed around Elbrus as incomplete eroded sections in the Tuzluk, Birjaly-su, and Nemetsky Aeroport localities, in the area of the Ullukol and Kukurtli glaciers, and the Irik-chat, Chuchkhur, and Chemartkol river basins. Two strata of rhyolites were distinguished [14,15] based on paleodose dating of quartz phenocrysts by electron paramagnetic resonance [15,16]. Recent efforts to perform high-accuracy zircon dating [17] of the lower rhyolite strata from various outcrops showed that they have the same age (1.98 Ma), which is close to the age of the Eldjurta granites (1.96 Ma) and older than magmatic activity at Elbrus. The upper rhyolites strata were formed 0.79–0.62 Ma [15] and were dated by [18] using U-Pb in zircons.

Lavas flows occur on the northern and southern slopes of the Elbrus volcano (K-Ar are < 0.2 Ma) [19], and separate volcanic vents (Tash-Tebe, Syltran, Tyzyl, Tashlysyrt) around Elbrus (K-Ar age 0.9–0.95 Ma) [20]. The lavas range in composition from basaltic trachyandesites to dacites; the least silicic lavas occur in peripheral lava flows [21].

3. Samples and Analytical Methods

Samples of young igneous rocks of the Greater Caucasus were collected in 2017 and 2019 by I.N. Bindeman, and were also previously collected by V.M. Gazeev and C. Gazis, the latter were stored and retrived from the Caltech repository. The collection included rhyolitic intracaldera and outflow tuffs of Chegem caldera (near Zayukovo village), Tyrnyauz rhyolitic lavas and granites, and Elbrus oldest rhyolitic tuffs (from the collections of Gazeev and Gurbanov) and dacitic lavas of the modern cone (Table S1). The same sample set was used for a U-Pb geochronological and isotopic study by [17]. The sampling sites are shown in Figure 1.

The composition of minerals and glasses was determined using a JEOL JXA-8230 microanalyzer and an Oxford X-Max^N energy-dispersive spectrometer with a detector area of 50 mm^2 (both Geological department of Lomonosov Moscow State University). The analysis of minerals composition was carried out at an accelerating voltage of 20 kV and a probe current of 10 nA (energy-dispersive spectrometer Oxford X-Max^N) or 30 nA (JEOL JXA-8230). The composition of volcanic glasses was determined at an accelerating voltage of 15 kV by a defocused electron beam 7 μm in diameter with a current of 7 nA, similar to the approach in [22]. Standards of natural silicates [23] and synthetic stoichiometric compounds were used as primary standards. The quality of the analysis was validated by repetitive measurements of natural standards (Smithsonian Institution) as a secondary test. Microprobe analyses of phenocryst minerals are included in the electronic Supplementary Materials.

The bulk rock composition was analyzed at the Vinogradov Institute of Geochemistry Siberian Branch of the Russian Academy of Science (Irkutsk, Russia). The bulk rock major element content was obtained using a sequential X-ray fluorescence spectrometer S4 Pioneer (Bruker AXS) according to the method for a sample of 500 mg [24]. The trace element concentration was determined by the method of mass spectrometry with ionization in inductively coupled plasma (ICP-MS) on a mass spectrometer with a magnetic sector ELEMENT 2 (Thermo Scientific) according to the method in [25]. Estimated precision (2SD) did not exceed 10 rel%. The quality was controlled by repetitive (every 5–6 measurements) analysis of two standards: BHVO-2 and AGV-2 (Table S2).

Oxygen isotope analysis was performed by laser fluorination at the University of Oregon using BrF5 as a reagent and a MAT253 mass spectrometer; most analyses were taken from the study of [17], and several new analyses were reported here.

Zircon dating was performed at ETH Zurich by LA-ICPMS, SHRIMP, and IDTIMS and described in the same study. We report one new LA-ICPMS date for Elbrus ignimbrite studied here that agrees with the previous date determination by [18]. A comprehensive U-Pb dataset for Elbrus will be presented by us shortly.

4. Results

4.1. Petrography and Mineralogy

4.1.1. Rhyolites of Chegem Caldera (2.9 Ma)

Rhyolites from Chegem caldera are dominantly vitroclastic tuffs, composed of pumice lithoclasts and crystal fragments in a matrix of small fragments of volcanic glass (Figure 2a). Phenocrysts in pumice fragments, individual crystals and their fragments are represented by quartz, sanidine, plagioclase, biotite, and titanomagnetite. Zircon, apatite, titanomagnetite, and allanite (containing up to 2 wt% ThO_2) are accessory phases. Plagioclase forms weakly zoned tabular crystals which are up to 2 mm long in the cross-section. Their composition varies in the narrow range of $An_{20}Ab_{73}Or_7$–$An_{27}Ab_{68}Or_5$ (Table S3). Prismatic crystals of apatite represent rare inclusions in plagioclase. Sanidine forms euhedral crystals, and their fragments are up to 2 mm in size. Weak zoning is typical to large crystals, characterized by a change in composition from $An_1Ab_{30}Or_{69}$ at the center to $An_1Ab_{40}Or_{59}$ at the edge of grains (Table S3). The composition of small sanidine crystals is similar to the outer parts of large phenocrysts. Biotite forms tabular crystals up to 0.5 mm in cross-sectional length and contains abundant zircon and apatite mineral contents. The biotite composition varies in the narrow range of Mg # = 43–47, 0.2–0.3 wt% MnO and 0.2–0.6 wt% Na_2O, 0.2–0.5 wt% F (Table S4). Quartz forms bipyramidal crystals which are up to 1.5 mm long. The composition of volcanic glass varies slightly from sample to sample and lies in the high silica range, 76.8–77.4 wt% SiO_2, 5.4–6.2 wt% K_2O (normalized to 100%). The measured oxide totals of volcanic glass are 95.1–97.6% (Table S5). The low totals are due to the presence of water (see Section 2). Crystals of titanomagnetite contain thin exsolution lamellae of ilmenite and are sporadically surrounded by a rim of pure magnetite with rare ilmenite crystals. The ilmenite lamellae are too small (<1–2 um) to analyze.

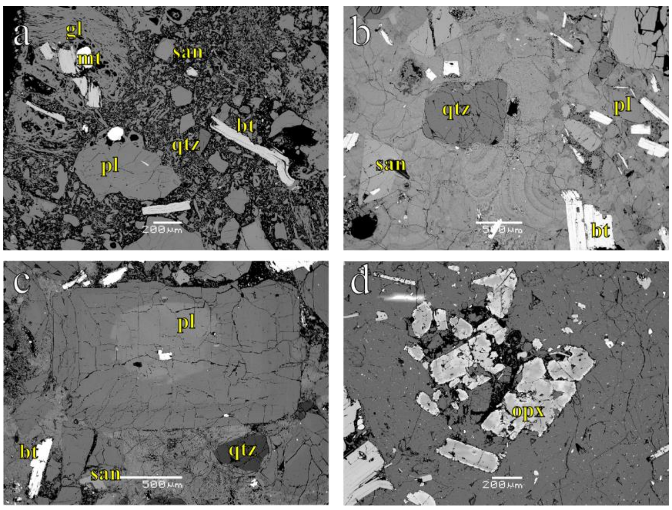

Figure 2. Backscattered electron (BSE) photographs of ignimbrites of the Chegem caldera (2.9 Ma) and early ignimbrites of Elbrus and rhyolites of Tyrnyauz (1.98 Ma). (**a**) Ignimbrite of the Chegem caldera, sample ELB-22; (**b**) Elbrus ignimbrite, sample ELB-12, (**c**) zoned plagioclase phenocryst from Elbrus ignibrite, sample ELB-13, (**d**) glomeroporphyric intergrowth of zoned orthopyroxene, biotite and plagioclase from Elbrus ignimbrite, sample ELB-9b. Phase abbreviations: pl—plagioclase, san—sanidine, bt—biotite, opx—orthopyroxene, qtz—quartz, mt—titanomagnetite, gl—volcanic glass.

4.1.2. Early (Lower) Rhyolites of Elbrus and Rhyolites of Tyrnyauz (1.98 Ma)

Elbrus area rhyolites sampled near the Tuzluk, Nemetsky Aeroport, and Kamennye Griby localities and rhyolites of the Tyrnyauz area have the same age, 1.98 Ma [17]. As we demonstrate here, these ignimbrites and rhyolitic necks are also identical in petrographic and mineralogical characteristics. They contain 20–30% of the crystals (Figure 2b) in welded and laminated high-silica rhyolitic glass. Euhedral phenocrysts (sometimes occurring as lithoclasts and individual crystals and fragments of plagioclase, biotite, sanidine, and quartz are present in glass. Plagioclase is predominantly represented by large (up to 1.5 mm) weakly zoned tabular crystals and their fragments (Figure 2c). Ignimbrite sampled at the base of the section of the upper ignimbrite strata in the Kamennye Griby area (sample ELB-11) contains individual crystals with a "spongy" core containing multiple fluid and mineral inclusions. The composition of plagioclase varies from $An_{51}Ab_{47}Or_2$ in the central parts of the crystals to $An_{23}Ab_{71}Or_6$ in the edge (Table S3). Sanidine is represented by large, predominantly unzoned, or weakly zoned crystals or their fragments with a composition in the range of $An_1Ab_{17–28}Or_{70–82}$ (Table S3).

Biotite forms tabular phenocrysts up to 0.5 mm in size, forms inclusions in quartz and plagioclase phenocrysts, and contains numerous inclusions of apatite and zircon. The largest grains are weakly zoned, although the composition of biotite generally lies in a narrow range of Mg # = 42–53, with contents of 0.1–0.4 wt% MnO, 0.2–0.6 wt% Na_2O, and 0.4–2 wt% F (Table S4). Quartz forms euhedral grains with evidence of minor pre-eruptive dissolution (slightly rounded crystal outlines). Orthopyroxene is scarce, and forms zoned crystals up to 0.3 mm in length in samples ELB-9, ELB-9b, and ELB-11 (Figure 2d). It is found in crystal clots with plagioclase or biotite, or occurs as separate phenocrysts. The zoning is characterized by a decrease in Mg# to the crystal margins (Mg# = 82–50), and variations of Cr_2O_3 content in the range of 0–0.32% (Table S6). Groundmass consists of fine-grained quartz-feldspar aggregate, sometimes forming spherulite textures. The pore space is filled with a silica phase, presumably vapor-deposited cristobalite or tridymite. Volcanic glass is found only in ignimbrites sampled at the top of the section in Kamennye Griby area (samples ELB-9, ELB-9b), where it is preserved inside lenticular fiamme. The composition of volcanic glass lies in the high-silica range 77–77.4% SiO_2, 6.4–6.6% K_2O (Table S5). Ilmenite (X_{Hem} = <5 mol%) and pyrrhotite are present as accessory phases.

4.1.3. Late (Upper) Rhyolites of Elbrus

The mineralogical features of Elbrus ignimbrites occurring in the base and west of the modern edifice are described based on three samples of the youngest (0.6–0.7 Ma) ignimbrites of the western slope of Elbrus. The zircon age from one of them (sample 55-1/97) was determined by LA_ICPMS in Zurich as 0.704 ± 0.017 Ma (n = 63, MSWD = 3.56). The presence of young (0.8–0.6 Ma) ignimbrites was noticed by Gurbanov [26] and described by Koronovskiy [13] in the western slope of Elbrus. Young ignimbrites are dense, lenticularly banded, and composed of welded lithic and crystal clasts (Figure 3a,b). The textural diversity mainly arises from the difference in crystallinity of lithoclasts and the degree of alteration of the rock matrix. The phenocryst association is represented by plagioclase, sanidine, quartz, biotite, and orthopyroxene. Plagioclase, which is present mainly as crystal fragments reaching 0.5 mm in length, has complex zoning with normal and reverse zones. Plagioclase composition varies over a wide range, $An_{46}Ab_{52}Or_2$–$An_{24}Ab_{71}Or_5$. Sanidine forms euhedral crystals with a composition in the range of $An_1Ab_{40}Or_{59}$–$An_1Ab_{27}Or_{72}$ (Table S3). Euhedral biotite crystals have the composition Mg # = 52–61, 0.1–0.15 wt% MnO and 0.55–0.8 wt% Na_2O, 0.8–3.5 wt% F (Table S4). Accessory minerals are represented by apatite, zircon, and ilmenite (X_{Hem} = 5–13 mol%).

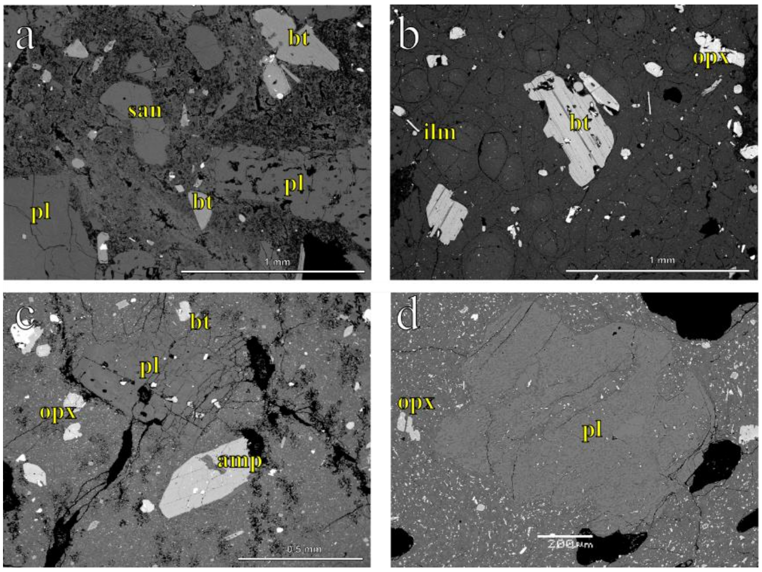

Figure 3. Back-scattered electron (BSE) photographs of young ignimbrites (0.7 Ma) and lavas (<0.25 Ma) of Elbrus. (**a**) Young Elbrus ignimbrite, sample 74k; (**b**) young Elbrus ignimbrite, sample 55-1/97; (**c**) Elbrus lava with phenocrysts of plagioclase, amphibole, biotite, and orthopyroxene, sample ELB-10; (**d**) "spongy" phenocryst of plagioclase in Elbrus lava, sample ELB-14. Phase abbreviations: pl—plagioclase, amp—amphibole, bt—biotite, opx—orthopyroxene, ilm—ilmenite.

4.1.4. Dacitic Lavas of Elbrus

Dacitic lavas of the modern Elbrus edifice (stage 5 according to the [15], Upper Pleistocene-Holocene) are dense, rarely moderately porous, homogeneous, or banded, with phenocrysts of plagioclase, biotite, amphibole, and orthopyroxene immersed in microlithic groundmass (Figure 3). Plagioclase phenocrysts up to 0.5 mm in size are strongly resorbed. They are represented either by crystals with resorbed cores with thin normally zoned mantle or crystals in which the oligoclase core is surrounded by a resorption zone, which has a thin normally zoned mantle. The composition of plagioclase in lavas ranges from $An_{28}Ab_{67}Or_5$ to $An_{63}Ab_{36}Or_1$ (Table S3). The biotite phenocrysts are almost unzoned, reaching a size of 0.3 mm, and are surrounded by a breakdown rim. Biotite is characterized by Mg # = 58–75, and contains 0.05–0.2 wt% MnO, 0.6–0.1 wt% Na_2O, and 0.6–2 wt% F (Figure 4, Table S4). Amphibole occurs as separate small (up to 0.2 mm) phenocrysts or rims on orthopyroxene crystals (Table S8). Orthopyroxene forms phenocrysts of various sizes (0.1–0.4 mm) with normal and reverse zoning. The most magnesian composition of orthopyroxene is characterized by Mg # = 88.1, the content of 4% Al_2O_3, 0.6% Cr_2O_3, and 0.2% MnO, and the most ferrous is characterized by Mg # = 50, the content of 0.5% Al_2O_3, <0.1% Cr_2O_3, and 1.2% MnO. (Figure 5, Table S6). Augite (Mg # = 71.6–80.6) is rare in the studied lavas; it is found only in samples (ELB-14, ELB-16, ELB-18) in a minor amount (Table S7). Apatite, titanomagnetite, and ilmenite (X_{Hem} = 9–35 mol%) are found as accessories. The microlithic fine-grained groundmass consists of plagioclase, pyroxenes, ilmenite, magnetite, and accessory apatite immersed in volcanic glass. The small size of microlites does not allow quantitative characterization of their composition.

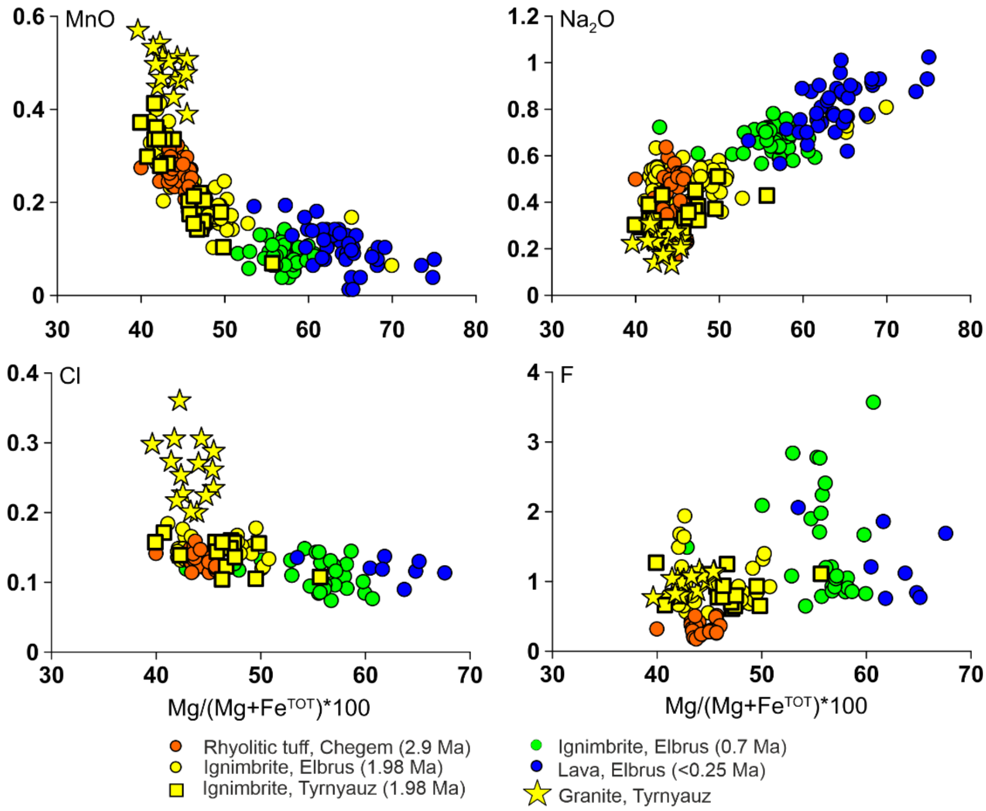

Figure 4. Composition of biotite phenocrysts in ignimbrites of the Chegem caldera, ignimbrites and lavas of Elbrus, and Eldjurta granites. The content of MnO, Na_2O, F, and Cl is given in wt%, Mg/(Mg + Fe^{TOT}) is calculated from atomic ratios.

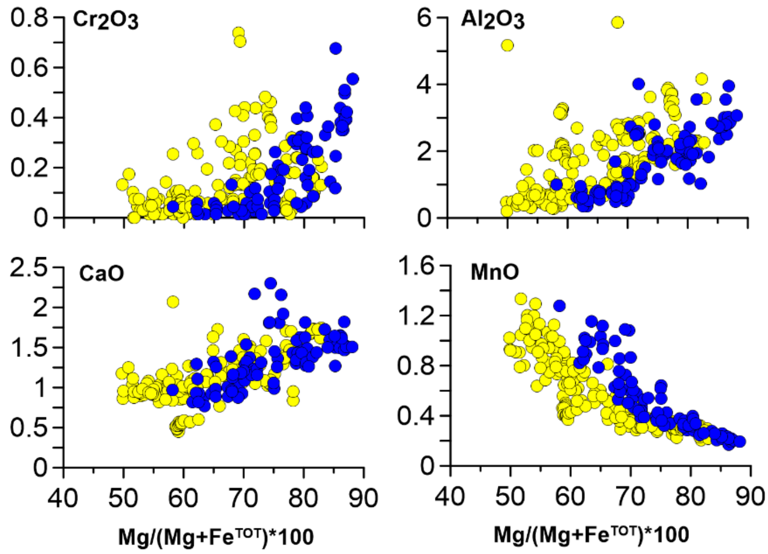

Figure 5. Composition of orthopyroxene phenocrysts in ignimbrites (1.96 and 0.7 Ma) and Elbrus lavas. Orthopyroxene from ignimbrites is shown in yellow, and lavas in blue. The content of Cr_2O_3, Al_2O_3, MnO, and CaO is given in wt%, Mg/(Mg + Fe^{TOT}) is calculated from atomic ratios.

4.1.5. Eldjurta Granite (Tyrnyauz)

The composition of the mineral phases of Eldjurta granite was characterized in one typical sample dated to 1.96 Ma [17] for comparison to the volcanic rocks. Only the compositions of biotite and ilmenite were determined. Biotite is characterized by Mg # = 39–45, 0.38–0.59 wt% MnO, 0.1–0.3 wt% Na_2O, 0.8–1.1 wt% F (Table S4). Ilmenite is characterized by a low content of the hematite endmember (X_{Hem} = 1–6 mol%).

4.2. Bulk Rock Composition

Bulk rock composition (Table S9) reveals that the studied rocks form compositional groups according to their age (Figure 6). The rhyolites of the Chegem caldera are the most silicic (73–75 wt% SiO_2), enriched in K_2O (4.2–4.7 wt%), and the most depleted in compatible elements—CaO, MgO, FeO, TiO_2, Al_2O_3, and P_2O_5 (Figure 6). Early ignimbrites of the Elbrus region (1.98 Ma), rhyolites, and granites of Tyrnyauz form another compositional group, which is less silicic (70.6–72% SiO_2) and less potassic (3.8–4.7 wt% K_2O) and enriched in CaO, MgO, FeO, TiO_2, Al_2O_3, and P_2O_5. Young ignimbrites (0.7 Ma) and young lavas of Elbrus are the least silicic (66.1–68 wt% SiO_2) and the most enriched in compatible elements (Figure 6).

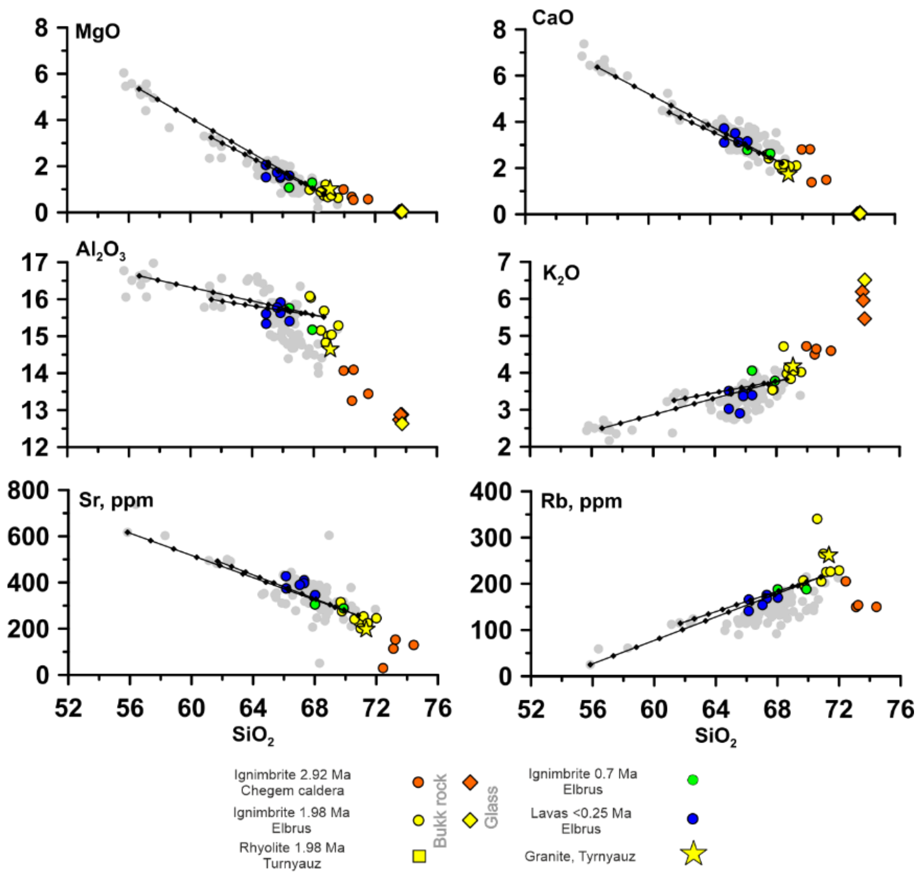

Figure 6. Bulk rock major element (in wt%), Rb and Sr (in ppm) content in ignimbrites of the Chegem caldera, ignimbrites and lavas of Elbrus and Eldjurta granites, and in rhyolitic matrix glasses. The gray circles show the published compositions of the Elbrus rocks [15,18,21,27,28]. Black lines show the modelled mixed compositions of the average composition of Elbrus ignimbrites with two compositions from the group of the least silicic lavas of the Elbrus region [21]. Diamonds on the lines correspond to compositions with a mixing ratio step of 10 wt%.

All studied rocks have negative Nb and Ta and positive Li, Pb, and K anomalies (Figure 7). The trace element distribution shows similarity among all young volcanic rocks and granites. The rhyolites of the Chegem caldera have the most pronounced negative anomalies in Nb, Ta, Sr, P, Zr, Hf, Eu, and Ti. The vitroclastic extracaldera tuff of the early eruption phase, overlapping with Jurassic carbonate rocks (sample ELB-25), exhibits the most prominent negative anomalies in the content of these elements, indicating fractionation of feldspar, apatite, and zircon. The early ignimbrites of Elbrus and the rhyolites of Tyrnyauz and Eldjurta granites have almost identical compositions. They are approximately twice enriched in Rb, Cs, U, Pb, Nb, and Ta and have higher concentrations of Sr, Ti, Ni, Cr, Co, V, Zn, Y, HREE, Li, Be, Sc, and Ga (Figure 8) compared to the Chegem ignimbrites. A characteristic feature of Chegem rhyolites is 1.1–1.2 times higher concentrations of K, Ba, Th, La, and Ce compared to the rhyolites, ignimbrites, and granites of Elbrus and Tyrnyauz. Late ignimbrites and lavas of Elbrus form a compositional trend, characterized by the progressive depletion of Cs, Rb, Th, U, Nb, Ta, P, HREE, Li, and Be, and an enrichment in Sr, LREE, Ti, V, Cr, Ni, and Co (Figure 8). Compared to island arc basalts (IAB), all young igneous rocks of the Greater Caucasus share a calc-alkaline to alkaline specification. However, they are more depleted in HREE, have more pronounced positive anomalies in Li and Pb, U and Th, and are also characterized by a higher enrichment in Th relative to U (Th/U = 3.2–5). All silicic rocks correspond to the I-type of granites due to their alumina saturation index (ASI < 1.05) and Th and U contents [29].

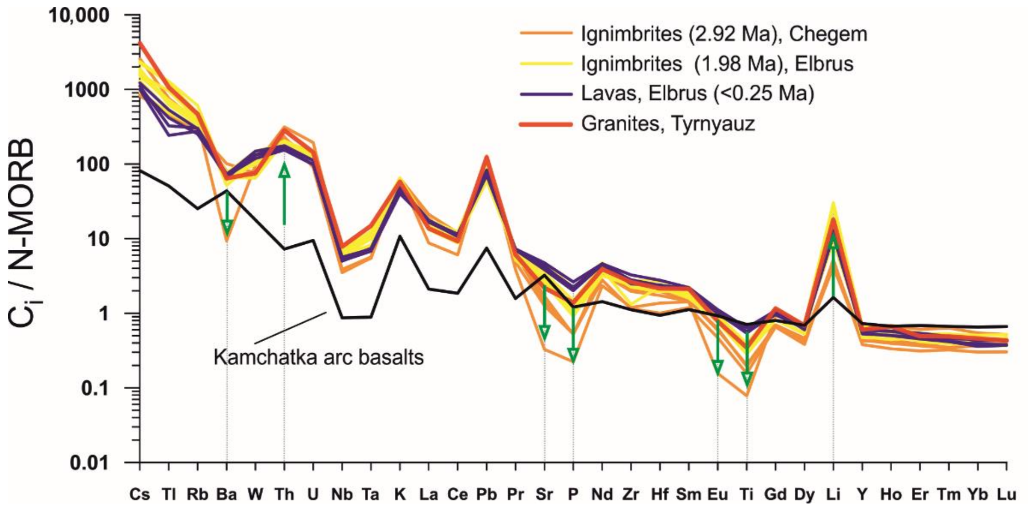

Figure 7. Trace element distribution (normalized to N-MORB) in ignimbrites of the Chegem caldera (orange lines), ignimbrites (yellow lines), and lavas (blue lines) of Elbrus and Eldjurta granites (red line). The average composition of the island arc basalts of the eastern volcanic front of Kamchatka is plotted for comparison [30]. Green arrows indicate the relative enrichment/depletion.

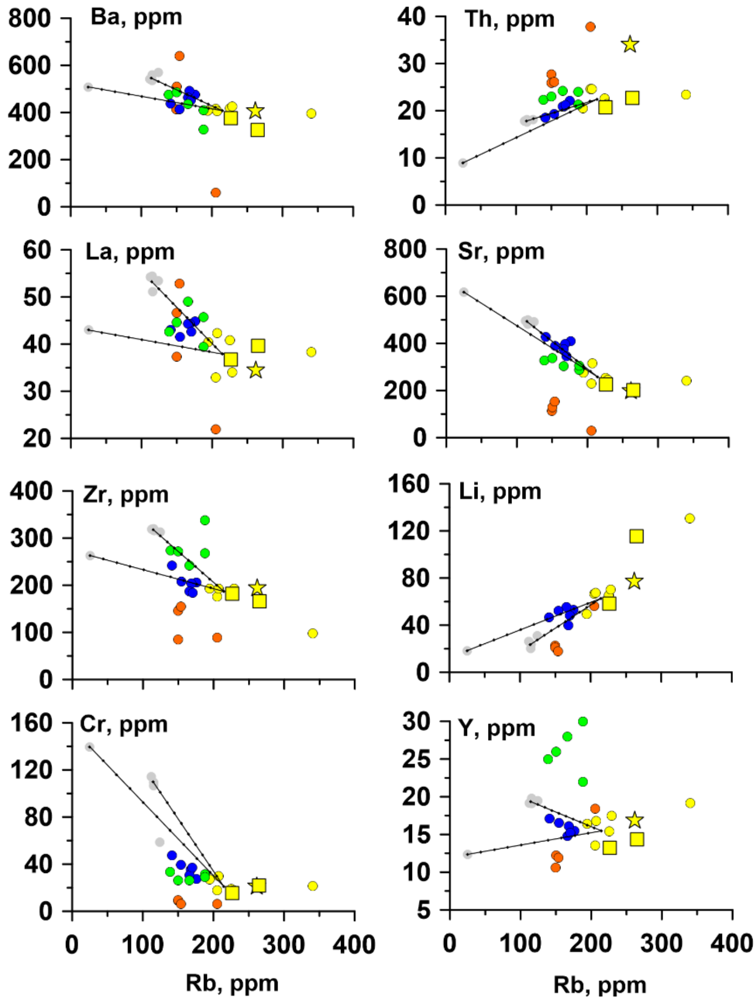

Figure 8. Trace elements content (in ppm) in ignimbrites of the Chegem caldera, ignimbrites and lavas of Elbrus, rhyolites of Tyrnyauz, and Eldjurta granites. The symbols are the same as in Figure 4. Gray circles show the compositions of the least silicic lavas of Elbrus. Black lines show the model compositions of mixing the average composition of Elbrus ignimbrites with two compositions from the group of the least silicic young lavas of the Elbrus region [21]. Diamonds on the lines correspond to compositions with a mixing step of 10 wt%.

4.3. Oxygen Isotopic Composition

The oxygen isotopic composition of plagioclase and quartz phenocrysts from young Elbrus ignimbrites is shown in Table S10. The oxygen isotopic composition in quartz shows similar values ($\delta^{18}O$ = 9.02–9.16) for three samples of young ignimbrites, corresponding to $\delta^{18}O$ values for magma in the 8.38–8.62 range of other Greater Caucasus magmas. Isotopic data for other young samples were previously determined by [17,31].

5. Discussion

5.1. Early Elbrus Rhyolites, Tyrnyauz Rhyolites, and Eldjurta Granites

Early rhyolites and ignimbrites of Elbrus, Tyrnyauz, and Eldjurta granites are similar in several petrographic and geochemical characteristics. The samples of granite and rhyolites are close in their major element (Figure 6) and trace element contents (Figure 7). The only significant difference is the elevated content of Th and Cs in Eldjurta granites. The rock-forming mineral assemblage and biotite composition are similar in all rocks studied here (Figure 4). Biotite in granites has slightly elevated MnO and Cl contents compared to ignimbrites and rhyolites, which can be explained by the accumulation of these elements in the melt during the late stages of granite crystallization and mark only the difference found in volcanic and plutonic products of the same magma. A remarkable feature is the relatively reduced crystallization conditions for early ignimbrites and Eldjurta granites (see below). Our data demonstrate the identity of the early Elbrus rhyolites, Tyrnyauz rhyolites, and Eldjurta granites. Along with the previously determined proximity of the Sr-Nd isotopic composition of rocks [28,32], the O-Hf isotopic composition of zircons and the same age [17], rhyolites (early Elbrus and Tyrnyauz) and Eldjurta granites must be considered as plutonic and volcanic derivatives of the same single (or extremely closely analogous) magma reservoir(s).

5.2. The 1.98 Ma Ignimbrites in the Basement of Elbrus Area and Chegem Rhyolites (2.9 Ma)

Compared to Chegem, the Elbrus and Tyrnyauz rhyolites are characterized by more calcic plagioclase, more potassic alkali felspar composition, elevated F content in biotite, and different accessory minerals, particularly Fe-Ti oxides. Elbrus and Tyrnyauz rhyolites are enriched in Rb, Cs, Zr, Y, Sr, U, Pb, Cr, Ti, Nb, Ca, and Mg, and slightly depleted in Th, Ba, La, and Ce compared to Chegem rhyolites (Figures 7 and 8). At the same time, the ratios of highly incompatible elements (Figure 9) and O-Sr-Hf isotopic composition (discussed below) are close for 1.98 and 2.9 Ma rhyolites, reflecting their genetic proximity. Higher content of incompatible elements and an increase in the fluorine content in biotite indicate that Elbrus and Tyrnyauz rhyolites may have been produced through crystal fractionation of Chegem magma between the 2.9 and 1.98 Ma volcanic impulses. Th, La, Ce, and Ba depletion is associated with the fractionation of allanite (concentrate Th and LREE) and alkali feldspar. An increase in the concentration of compatible elements points to the possibly significant role of assimilation, as discussed below.

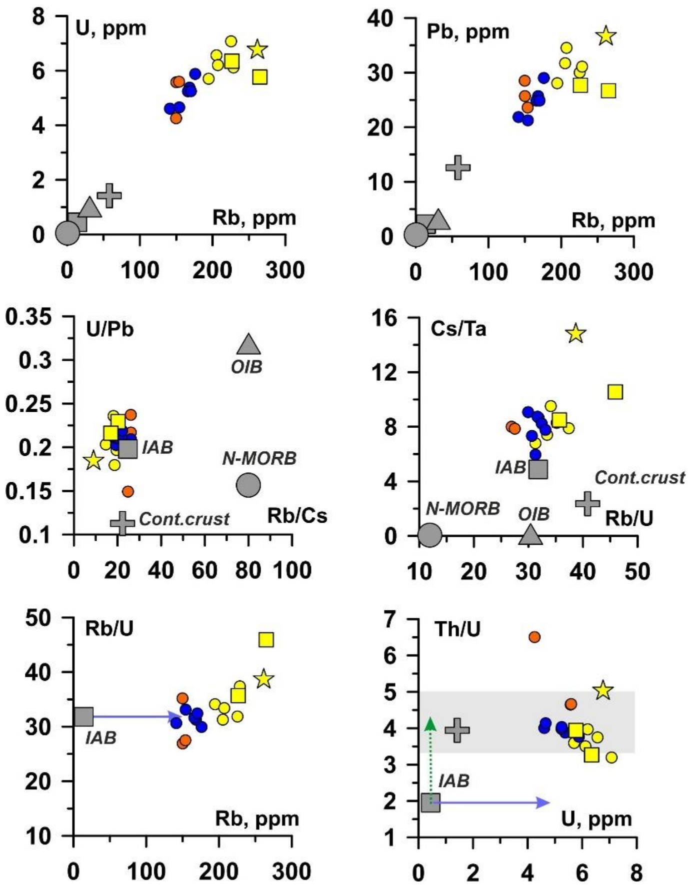

Figure 9. Bulk rock trace element contents and ratios in silicic young igneous rocks of the Greater

Caucasus compared to basalts of different geodynamic settings and the Earth's crust. Symbols for young igneous rocks of the Greater Caucasus are the same as in Figure 4. Additionally shown: gray square—average composition of island arc basalts of the eastern volcanic front of Kamchatka (IAB, [30]), gray circle—average composition of basalts of mid-oceanic ridges (N-MORB according to [33]), gray triangle—average composition of basalts of oceanic islands (OIB according to [33]), gray cross—average composition of continental crust [34]. Blue arrows—based on mass-balance calculations evolution of the elemental abundances and their ratios in during fractionation of 90% of crystals from the model island arc basalt. The calculations assume bulk mineral-melt partition coefficients to be equal: ${K_D}^{Rb}$ = ${K_D}^{Cs}$ = ${K_D}^{U}$ = ${K_D}^{Th}$ = 0. The green dashed arrow indicates the direction (not quantitively) of element ratios' evolution during supra-subduction mantle enrichment by sedimentary material. The gray area in the Th/U–U diagram illustrates the range of Th/U ratios in modern island arc rocks, where sediment flux is proposed [35].

5.3. Origin of Rhyolite Magmas of the Greater Caucasus

The geodynamic modeling by Bindeman et al. [17] suggested the origin and evolution of young magmatism in response to the melting of the delaminating supra-subduction lithosphere during the Caucasus orogeny. This model is consistent with the observed geophysical structure of the upper mantle and crust under the Greater and Lesser Caucasus [36,37].

We here utilize a geochemical approach to determine the nature of the magma source which traditionally uses ratios of highly incompatible elements. These ratios remain nearly constant during magma differentiation and reflect the nature of the melt source and melting conditions. Applying this approach to silicic magma is complicated because many traditionally incompatible elements become progressively compatible as some major minerals (e.g., sanidine) and accessory minerals (e.g., zircon, allanite, chevkinite) join the assemblage in highly differentiated rhyolitic magmas. We used Cs, Rb, U, Pb, and Ta to characterize the melt source, since ratios of these elements do not change significantly even in the most differentiated rocks studied here and worldwide (Figure 9). Moreover, Cs, Rb, and Ta remain "perfectly incompatible" as they are not included in significant quantities in the rock-forming and accessory minerals observed in the samples.

Generally, young volcanic rocks of the Elbrus, Tyrnyauz, and Kazbek areas are calc-alkaline, enriched in LILE such as Rb, Sr, Ba, U, and Pb, and depleted in HFSE, e.g., Ti, Zr, and Nb, as was established by previous research [9,28,38], which emphasized the close relationship of silicic magmatism with magma generation processes under supra-subduction conditions. Rhyolites of the Chegem caldera fall on the Rb vs. Y + Nb diagram [39] near the boundary between syn-collisional and volcanic arc granitoids [17,28].

Our new data in Figure 9 illustrates the ratios of incompatible elements in rhyolites, dacites, and granites. For comparison, the island arc basalts of the eastern volcanic front of Kamchatka [30] were taken as a model composition of island arc magmas, along with the compositions of N-MORB and OIB [33], and the average composition of the continental crust [34]. Young Great Caucasus silicic rocks are geochemically close to the island arc calc-alkaline basalts, suggesting that they are derivatives of supra-subduction basaltic magma, inheriting their geochemical characteristics from LILE rich subduction fluids. Furthermore, we used the average composition of the eastern volcanic front of Kamchatka IAB, an example of supra-subduction mantle-derived magmas formed under conditions of long-lived subduction of the mature oceanic lithosphere under the continent margin with a thick crust, as a proxy for parental basaltic magma.

The content of Rb, Cs, U, and Pb in ignimbrites of the Chegem caldera is approximately 5–10 times higher than their average content in other island arc basalts. This similar level of enrichment suggests that silicic magmas can nominally be produced by ~80–90% fractionation (assuming the incompatible behavior of Rb, U, and other incompatible elements K_D = 0) of crystals from island arc basalts (the role of assimilation is discussed below). Experimental data [40,41] show that dacitic and rhyolitic magmas can form at >80% of crystal fractionation in the presence of water under lower crustal conditions. Fractionation of basaltic magma in the lower crust under supra-subduction conditions can generate significant volumes of silicic magmas by melting [42,43]. The melting of crustal material would produce higher concentrations of incompatible elements in anatectic magmas because average crustal material has two to five times higher bulk concentrations than IAB.

Significant depletion of Chegem magmas in compatible elements—Mg, Ca, Sr, Ti, Ni, Cr, Co, V, Zn, and Y—in comparison with arc basalts requires fractionation of the association of plagioclase, Fe-Mg silicates and spinel (and/or titanomagnetite), which provides another supporting evidence for a high degree of fractionation. Thus, geochemical features of magmas that fed the volcanic activity of the Chegem caldera were produced by the fractionation of IAB-like magmas. The origin of isotopic composition is discussed in detail below.

5.4. Reasons for Th and U Enrichment and High Th/U Ratios

Unlike other incompatible elements, in particular, U, whose content is ~5–10 times higher than in model island arc basalts, the Th content in rhyolites and granites exceeds the concentration in island arc basalts by 25–40 times (av. 27 ppm). The average Th/U ratio is about 4, roughly corresponding to the crustal value (Th/U = 4.2). Such Th enrichment cannot be generated simply by crystal fractionation of basalts (which will be closer to 2.5–3), as we demonstrated for other incompatible elements, and requires an additional source of Th. Thorium enrichment may be attributed to crustal assimilation. However, during melting of metamorphic rocks, Th remains in restite, retained by accessory phosphates (monazite) [44], so we assume this scenario is unrealistic.

The enrichment of magmas in Th over other elements is known for some island arc magmas [45,46]. The melting of subducted sedimentary rocks enriched in insoluble Th, produced by the destruction of the mature crust, may lead to supra-subduction mantle fertilization and the production of magmas enriched in Th by up to 25 ppm (for basalts and andesites) [35]. The enrichment of supra-subduction magmas in Th leads to an increase in the Th/U ratio to 3.2–5, which overlaps with the values of this ratio for Chegem rhyolites (Th/U = 4.6) and rhyolites of Elbrus and Tyrnyauz (Th/U = 3.2–5). On the Th/Yb-Nb/Yb diagram (not shown), the compositions are significantly shifted from the MORB mantle array towards an increased Th/Yb ratio, indicating supra-subduction enrichment as well.

5.5. Origin of Isotopic Characteristics

Previous studies of the Sr-Nd isotopic composition of silicic rocks [28] of the Greater Caucasus and O-Hf isotopes in zircons [17] demonstrated evidence of a hybrid mantle-crustal origin of young magmatic rocks of the Greater Caucasus. The estimated crustal material in the volcanic rocks varies from 20% to 25% for Chegem rhyolites to 50% to 55% for early Elbrus rhyolites. This increasing role of crustal material between 2.9 and 1.98 Ma is likely caused by crust assimilation, which is also seen in trace elemental behavior. On the other hand, the incorporation of a significant amount of crustal material to Chegem magma contradicts the low abundance of incompatible elements. Zircon crystals in rhyolites form homogeneous populations with the presence of neither older nor geochemically distinct crystals [17]. This, together with relatively moderate (for collisional environment magmas) oxygen and strontium isotopic ratios, allows us to exclude melting Paleozoic differentiated crustal material as a source of silicic magma.

5.5.1. Role of Mantle Source Enrichment

An isotopic composition different from MORB in magmatic rocks is usually attributed to the melting of an enriched mantle or crustal source. Since crustal melting seems unlikely, we testify that the metasomatized supra-subduction mantle may produce observed isotopic ratios. The isotopic composition of the Chegem rhyolite magmas ($^{87}Sr/^{86}Sr$ = 0.7055–0.7076 [10], εHf = +1.7 to +5.6, and $\delta^{18}O$ from + 7‰ to + 8.6‰ [30]) overlaps with the characteristic range of supra-subduction magmas of modern mature island arc systems. Low εHf (0–3) values may be produced only by sediment admixture to a mantle wedge [47] without crust assimilation. Direct evidence isotopic sub-arc mantle enrichment ($\delta^{18}O$ = +8.03) is known for the peridotite xenolith from South Tibet [48].

Chegem rhyolites have Sr and Hf isotopic ratios far from the mantle values; at the same time, $\delta^{18}O$ is only slightly higher (for 2–3‰) than the typical mantle. Such isotopic patterns may be produced by isotopic mixing of two components, one of which is depleted in Sr and Hf [49], as in the case of supra-subduction enrichment of peridotite, and depleted in trace elements, by means of enriched fluid or melt from the subducting lithosphere.

Figure 10 illustrates the average Sr-Hf-O isotopic compositions of young Greater Caucasus rhyolites and granites (data from this work, [10,15,17,32,50]). The isotopic mixing lines model two scenarios: (1) isotopic MORB-like mantle ($\delta^{18}O$ = 5.8, εHf = 15, $^{87}Sr/^{86}Sr$ = 0.703, [51,52]) enrichment under supra-subduction conditions; (2) crustal assimilation by magma with MORB-like isotopic composition. Since Th/U and Th/Yb ratios of the studied rocks are shifted from MOBR-array, we assumed sediment incorporation in the magma generation zone (see section); we used Phanerozoic sediment isotopic composition as a mixing endmember proxy. Sediment isotopic composition is variable, so we chose values of $\delta^{18}O$ = 20, εHf = −5, $^{87}Sr/^{86}Sr$ = 0.71, which are within the variation ranges of observed oceanic sediments [53,54]. Variation of the model sediment composition within the natural range will not principally affect the interpretation. As shown in Figure 10, the isotopic compositions of rhyolites and granites are close to the mixing line corresponding to mantle enrichment, and indicate the addition of 10–20% of material with isotopic characteristics of modern sedimentary rocks (Figure 10).

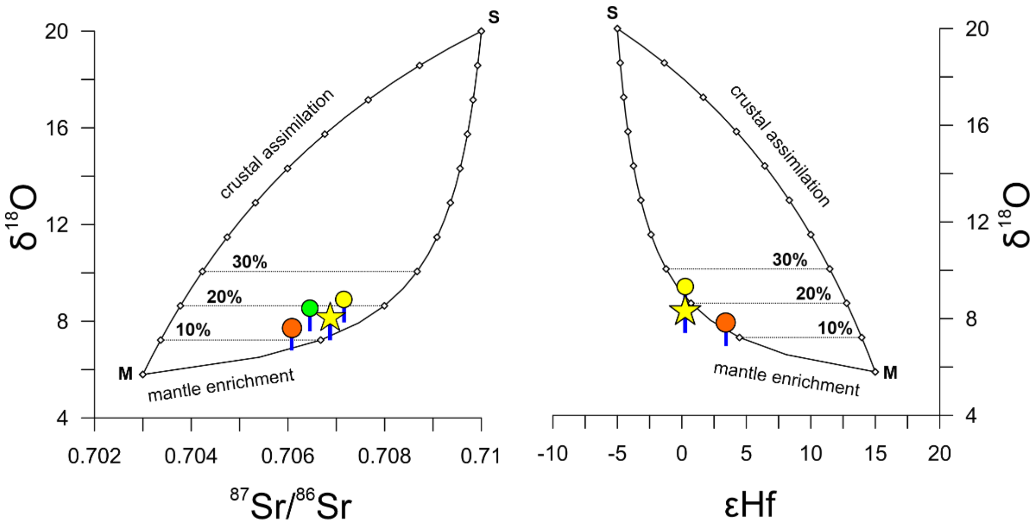

Figure 10. Average isotopic composition of Sr, Hf and O ignimbrites of the Chegem caldera (orange circle) and ignimbrites of Elbrus and Tyrnyauz (1.98 Ma—yellow circle, 0.7 Ma—green circle) and Eldjurta granites (yellow star). Isotopic mixing lines between the model compositions of the mantle (denoted by the symbol "m", isotopic composition—$\delta^{18}O$ = 5.8, εHf = 15, $^{87}Sr/^{86}Sr$ = 0.703) and sedimentary material (denoted by the symbol "s", isotopic composition—$\delta^{18}O$ = 20, εHf = −5, $^{87}Sr/^{86}Sr$ = 0.71) reflect two scenarios: enrichment of the mantle source under suprasubduction conditions ($Sr_{mantle}/Sr_{contaminant} = Hf_{mantle}/Hf_{contaminant}$ = 0.1) and magma assimilation of crustal matter ($Sr_{magma}/Sr_{contaminant} = Hf_{magma}/Hf_{contaminant}$ = 2). The blue lines show a potential increase in $\delta^{18}O$ by ~1‰ during fractional crystallization. The average strontium isotopic composition was taken from [10,38,50], and that of hafnium was taken from [31].

The isotopic composition of oxygen, unlike Sr and Hf, may increase insignificantly during fractional crystallization. However, fractionation from basalt to dacite with deep crustal pyroxene and amphibole fractionation and without plagioclase causes a maximum possible increase in $\delta^{18}O$ of 1–1.2‰ (summary in the work [55]). In the case of the early fractionation of plagioclase, isotopic fractionation does not exceed 0.4‰ [56]. Thus, the potential fractionation's effect on oxygen isotopic composition cannot explain the multi-permil range that we observe.

5.5.2. Role of Crustal Assimilation

Crust assimilation during magma evolution is clearly indicated by comparing the Hf-O isotopic ratios of Chegem and early Elbrus and Tyrnyauz rhyolites [31]. The latter was enriched with compatible (Ca, Mg, Al, Sr, Cr, Ni) and incompatible elements (Figure 8). Observed geochemical features indicate that Elbrus and Tyrnyauz magma were generated from magma compositionally similar to Cherem rhyolites through the crystallization and assimilation of wall rocks. Furthermore, we constrain this process using petrological and geochemical observations.

Magnetite-bearing Chegem rhyolites and granodiorites (also reported by [9]) contrast with ilmenite-bearing early Elbrus rhyolites Tyrnyauz granites in oxidizing conditions. Accessory Fe-Ti oxides are the main indicators of the redox conditions. Magnetite-bearing granites are more oxidized environments, while ilmenite-bearing are more reduced [57]. The transition between magnetite and ilmenite series approximately corresponds to the NNO buffer [58]. Rhyolites of the Chegem caldera and their cogenetic granodiorites contain titanomagnetite [9], indicating relatively oxidized conditions. Ilmenite in these rocks occurs only in the form of small rare segregations along titanomagnetite grain edges. Early ignimbrites of Elbrus, rhyolites, and granites of Tyrnyauz, the next major stage of magmatic activity, are additionally characterized by the paragenesis of pyrrhotite and ilmenite with a very low content of the hematite endmember (X_{Hem} = 0–5 mol%), indicating a change in redox conditions. Experiments in a rhyolitic water-saturated system [59] reproduce pyrrhotite in the temperature range of 800–1000 °C only at low oxygen fugacity, corresponding to NNO oxygen buffer or lower. Reduced ilmenite-bearing silicic rocks in collisional settings are traditionally associated with the incorporation of organic carbon from sedimentary (or metasedimentry) rocks [57]. The reducing fO_2 may indicate assimilation of sedimentary rocks. Potential candidates include Paleozoic and Mesozoic volcanogenic-sedimentary and terrigenous-sedimentary rock, which contain sporadic coal strata.

The euhedral phenocrysts in rhyolites (both Chegem and early Elbrus), the absence of microlites, and the similar composition of matrix glass and melt inclusions published by Babanskiy, Tolstykh and their coauthors [60,61] suggest that magmas did not experience any significant crystallization during the syn-eruptive evacuation to the surface, which is probably associated with the rapid loss of water and glass quenching, as observed in Yellowstone lavas [62]. Thus, matrix glass may be used as a direct proxy for pre-eruptive melt composition (Figure 11) at storage. On a Q-Pl-Kfs projection melt composition shifted to higher potassium relative to the polybaric line of temperature minima for a water-saturated haplogranite system [63]. Experimental studies show that such a shift in melt composition, in equilibrium with quartz and feldspars toward potassic compositions, occurs either at water activity <1, as in the case of the mixed water-carbon dioxide fluids [64], or at fluid undersaturated conditions [65]. Low water activity, which is likely due to the presence of carbon dioxide, may indicate the assimilation of carbon-bearing sedimentary material, whether this be organic matter, limestone, or both. Carbon and oxygen isotopes around the carbonate inclusions abundant in the Chegem ignimbrites indicate the volatilization of organic carbon [17], so some of these processes do occur at least near the surface.

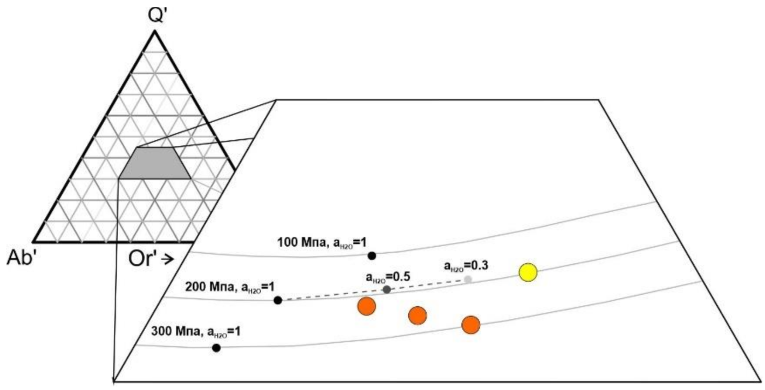

Figure 11. Average compositions of unaltered matrix glasses of the bulk of ignimbrites of the Chegem caldera (2.92 Ma) and Elbrus (1.98 Ma) projected following the algorithm of Blundy and Cashman [66] for the haplogranite triangle. The positions of the quartz-feldspar cotectic lines and the thermal minima at P = P_{H2O} (aH_2O = 1) are taken from the work of Tuttle and Bowen [63] and the position of the thermal minima for 200 MPa and aH_2O < 1 is taken from the work of Ebadi and Johannes [64].

5.6. Origin of Young Ignimbrites and Lavas of Elbrus Area

Young 0.7 Ma Elbrus ignimbrites and lavas of the Elbrus cone share common petrological and geochemical features. Successive depletion in silica and enrichment in Ca, Mg, Cr, and other elements indicate their formation as a result of mixing of rhyolitic and mafic magma (Figures 6 and 8). Bulk composition, the mineral assemblage and composition gradually change from Pl-Kfs-Q-Opx-Bt in rhyolites to Pl-Opx-Amp-Bt in lavas; biotite and orthopyroxene become more Mg-rich. The presence of "spongy" crystals of plagioclase, zoned phenocrysts of orthopyroxene and plagioclase indicates the mixing of compositionally contrasting magmas. Within individual zones of orthopyroxene, its Mg# reaches 88 mol%, and its Cr_2O_3 content reaches 0.7 wt%. This indicates that admixed magma had a basic composition. The increase in admixed mafic magmas is confirmed by isotopic data, which demonstrate an increase in εHf values and a decrease in $\delta^{18}O$ from early to late ignimbrites and lavas of Elbrus. Basaltic lavas near the Elbrus are relatively rare, which indicates that the mafic magmas of the late stage of the volcanic center's development may have been trapped by a silicic magma chamber. The least silicic young lavas near Elbrus are basaltic trachyandesites effused from monogenic volcanic edifices on the periphery of the modern Elbrus volcanic edifice [21]. Since young ignimbrites and lavas of Elbrus are close to the mixing line between Elbrus and Tyrnyauz rhyolite and basaltic trachyandesite, the latter may be a good proxy for the composition magmas which fed effusive activity in a final stage (Figures 6 and 8). Mass-balance calculation suggests admixing of at least 40–50% basaltic trachyandesite to reproduce the composition of dacitic lavas. It is also possible that differentiate of these more mafic magmas mixed with resident dacites. At the same time, isotopic data indicate that the fraction of "crustal" material in early ignimbrites is only 5–10% higher than that in young lavas, which may indicate that the main magmas of the late volcanism of Elbrus volcano also have crustal isotopic characteristics, and their origin can be traced to a common silicic magma body formed 0.7 Ma.

Basaltic trachyandesite and andesite lavas erupted 690–830 (±50) thousand years ago in the area around Elbrus, namely the Tash-Tebe volcanic apparatus, and 950–900 (±50) ka for the Tyzyl, Tashlysyrt, and Syltran volcanic edifices [20]. According to this dating, young ignimbrites (700 thousand years old) and lavas of the stratovolcanic edifice of Elbrus, studied by us and other authors [15,27], erupted after the formation of monogenic mafic volcanic edifices. In a numerical geodynamic model of Caucasus collision [17] a significant basaltic magmatism pulse occurred 0.5–0.7 Ma ago, suggesting temporal compatibility of the model with the observed record.

6. Conclusions

The young silicic magmatism of the Greater Caucasus, including Chegem rhyolites, Tyrnyauz, early and late Elbrus rhyolites, Eldjurta granites, and Elbrus dacitic lavas, has similar island arc-like geochemical characteristics. Shared close ratios of highly incompatible elements indicate that all silicic rocks were produced as a result of the development of a long-lived crustal magmatic system. The evolution of the major and trace element contents and mineral and isotopic compositions of silicic magmas allowed us to propose a unified scheme of collisional magmatism development.

The relatively low contents of incompatible element ratios, $\delta^{18}O$ and $^{87}Sr/^{86}Sr$ values for collisional settings suggest that Chegem rhyolitic magma could be generated by 80–90% fractional crystallization of mantle-derived basalts with island arc geochemical affinity. The observed O-Sr-Hf isotopic composition and the elevated Th/U ratios could be derived from the sub-arc mantle, fertilized by sediment-derived melts of fluids.

Mineralogically and geochemically similar early Elbrus ignimbrites, Tyrnyauz rhyolites and Eldjurta granites were likely formed from Chegem-like magma through the fractional crystallization and assimilation of crustal rocks. The observed mineralogical and geochemical features suggest that assimilants were likely represented by sedimentary or volcano-sedimentary carbonate-bearing rocks, which are present nearby.

Further evolution of the magmatic system, as captured by late Elbrus ignimbrites and lavas of the modern stratovolcanic edifice, is driven by the mixing of the rhyolitic magma reservoir with more mafic magmas, which is close in composition to basaltic trachyandesites, which occur as lava flows at the periphery of Elbrus volcano.

Supplementary Materials: The following supporting information can be downloaded at: https://www.mdpi.com/article/10.3390/min12010105/s1, Table S1: Sample description; Table S2: Results of ICP-MS measurements of BHVO-2 and AGV-2 standards; Table S3: Composition of feldspar phenocrysts; Table S4: Composition of biotite phenocrysts; Table S5: Composition of matrix glass; Table S6: Composition of orthopyroxene phenocrysts; Table S7: Composition of clinopyroxene phenocrysts; Table S8. Composition of amphibole; Table S9: Bulk rock composition; Table S10: Oxygen isotope composition of young Elbrus ignimbrites.

Author Contributions: Conceptualization, I.B.; methodology, V.S. and I.B.; formal analysis, V.S. and I.B.; investigation, V.S. and I.B.; resources, I.B., V.S. and V.G.; data curation, V.S.; writing—original draft preparation, V.S.; writing—review and editing, I.B. and V.G.; visualization, V.S.; supervision, I.B.; project administration, I.B.; funding acquisition, I.B. All authors have read and agreed to the published version of the manuscript.

Funding: This research was funded by RUSSIAN SCIENCE FOUNDATION, grant number 19-17-00241; V.S. acknowledges support from M.V. Lomonosov Moscow State University Program of Development.

Data Availability Statement: Not acceptable.

Acknowledgments: The authors are grateful to S. Popov, N. Nekrylov, and O. Melnik for their help during fieldwork. A.B. Perepelov for major and trace element analyses, M. Guillong for one U-Pb age. We acknowledge the efforts of four anonymous reviewers, which significantly improved the manuscript.

Conflicts of Interest: The authors declare no conflict of interest.

References

1. Pearce, J. Sources and settings of granitic rocks. *Episodes* **1996**, *19*, 120–125. [CrossRef]
2. Moyen, J.-F.; Laurent, O.; Chelle-Michou, C.; Couzinié, S.; Vanderhaeghe, O.; Zeh, A.; Villaros, A.; Gardien, V. Collision vs. Subduction-Related Magmatism: Two Contrasting Ways of Granite Formation and Implications for Crustal Growth. *Lithos* **2017**, *277*, 154–177. [CrossRef]
3. France-Lanord, C.; Le Fort, P. Crustal Melting and Granite Genesis during the Himalayan Collision Orogenesis. *Earth Environ. Sci. Trans. R. Soc. Edinb.* **1988**, *79*, 183–195. [CrossRef]

4. Azizi, H.; Asahara, Y. Juvenile Granite in the Sanandaj–Sirjan Zone, NW Iran: Late Jurassic–Early Cretaceous Arc–Continent Collision. *Int. Geol. Rev.* **2013**, *55*, 1523–1540. [CrossRef]
5. Li, X.; Li, W.; Wang, X.; Li, Q.; Liu, Y.; Tang, G. Role of Mantle-Derived Magma in Genesis of Early Yanshanian Granites in the Nanling Range, South China: In Situ Zircon Hf-O Isotopic Constraints. *Sci. China Ser. D Earth Sci.* **2009**, *52*, 1262–1278. [CrossRef]
6. Soesoo, A. Fractional Crystallization of Mantle-Derived Melts as a Mechanism for Some I-Type Granite Petrogenesis: An Example from Lachlan Fold Belt, Australia. *J. Geol. Soc.* **2000**, *157*, 135–149. [CrossRef]
7. Minanovskiy, E.E.; Koronovsky, N.V. *Orogenic Volcanism and Tectonics of the Alpine Belt of Eurasia*; Nauka: Moscow, Russia, 1973.
8. Grün, R.; Tani, A.; Gurbanov, A.; Koshchug, D.; Williams, I.; Braun, J. A New Method for the Estimation of Cooling and Denudation Rates Using Paramagnetic Centers in Quartz: A Case Study on the Eldzhurtinskiy Granite, Caucasus. *J. Geophys. Res. Solid Earth* **1999**, *104*, 17531–17549. [CrossRef]
9. Lipman, P.W.; Bogatikov, O.A.; Tsvetkov, A.A.; Gazis, C.; Gurbanov, A.G.; Hon, K.; Koronovsky, N.V.; Kovalenko, V.I.; Marchev, P. 2.8-Ma Ash-Flow Caldera at Chegem River in the Northern Caucasus Mountains (Russia), Contemporaneous Granites, and Associated Ore Deposits. *J. Volcanol. Geotherm. Res.* **1993**, *57*, 85–124. [CrossRef]
10. Gazis, C.A. An Isotopic Study of the Fluid Flow and Thermal History of the 2.8 Ma Chegem Ash-Flow Caldera and Related Intrusive Rocks. Ph.D. Thesis, California Institute of Technology, Caucasus Mountains, Russia, 1995.
11. Myshenkova, M.S. Geological Position, Composition, Age and Genesis Pliocene-Quaternary Silicic Volcanics of Elbrus Volcanic Region (North Caucasus). Ph.D. Thesis, Moscow State University, Moscow, Russia, 2021.
12. Kostitsyn, Y.A.; Kremenetsky, A.A. Age of Final Magmatic stage of the Eldjurtu Granite: Rb–Sr Isochron Dating of Aplites. *Geokhimiya* **1995**, *7*, 925–932.
13. Koronovsky, N.V.; Myshenkova, M.S. Structure of the western slope of Elbrus volcano and Elbrus area. *Geol. Geophys. South Russ.* **2016**, *6*, 60–73.
14. Bogatikov, O.A.; Gurbanov, A.G.; Koshchug, D.G.; Gazeev, V.M.; Shabalin, R.V.; Dokuchaev, A.Y.; Melekestsev, I.V.; Sulerzhitskii, L.D. Main Evolutionary Phases of Elbrus Volcano (Northern Caucasus, Russia) Based on EPR Dating of Quartz. *J. Volcanol. Seismol.* **2003**, *3*, 3–14.
15. Gazeev, V.M. *Petrology and Potential Ore Prospects of Elbrus Volcanic Center. Extended Abstract of Cand Sci (Geol-Miner)*; IGEM RAS: Moscow, Russia, 2003.
16. Koshchug, D.G.; Solovyov, Y.P. Accumulation of Structural Radiation Defects in Quartz in Cooling Systems: Basis for Dating. *Phys. Chem. Miner.* **1998**, *25*, 242–248. [CrossRef]
17. Bindeman, I.N.; Colón, D.P.; Wotzlaw, J.-F.; Stern, R.; Chiaradia, M.; Guillong, M. Young Silicic Magmatism of the Greater Caucasus, Russia, with Implication for Its Delamination Origin Based on Zircon Petrochronology and Thermomechanical Modeling. *J. Volcanol. Geotherm. Res.* **2021**, *412*, 107173. [CrossRef]
18. Gurbanov, A.G.; Gazeev, V.M.; Bogatikov, O.A.; Dokuchaev, A.Y.; Naumov, V.B.; Shevchenko, A.V. Elbrus Active Volcano and Its Geological History. *Russ. J. Earth Sci.* **2004**, *6*, 257–277. [CrossRef]
19. Lebedev, V.A.; Bubnov, S.N.; Chernyshec, I.V.; Medvedeva, E.S. Chronology of Magmatic Activity of the Elbrus Volcano (Greater Caucasus): Evidence from K–Ar Isotope Dating of Lavas. *Dokl. Earth Sci.* **2005**, *405A*, 1321–1326.
20. Lebedev, V.A.; Bubnov, S.N.; Yakushev, A.I. Magmatic Activity within the Northern Caucasus in the Early Neopleistocene: Active Volcanoes of the Elbrus Center, Chronology, and Character of Eruptions. *Dokl. Earth Sci. Springer Nat. BV* **2011**, *436*, 32. [CrossRef]
21. Gazeev, V.M.; Gurbanov, A.G.; Gurbanova, O.A. Moderately alkaline basaltic andesite and andesites of the Elbrus volcanic district (North Caucasus): Questions petrogenesis, geodynamic typification and geochemical specialization. *Geol. Geophys. South Russ.* **2019**, *9*, 40–55.
22. Ponomareva, V.; Polyak, L.; Portnyagin, M.; Abbott, P.M.; Zelenin, E.; Vakhrameeva, P.; Garbe-Schönberg, D. Holocene Tephra from the Chukchi-Alaskan Margin, Arctic Ocean: Implications for Sediment Chronostratigraphy and Volcanic History. *Quat. Geochronol.* **2018**, *45*, 85–97. [CrossRef]
23. Jarosewich, E.; Nelen, J.A.; Norberg, J.A. Reference Samples for Electron Microprobe Analysis. *Geostand. Newsl.* **1980**, *4*, 43–47. [CrossRef]
24. Amosova, A.A.; Panteeva, S.V.; Tatarinov, V.V.; Chubarov, V.M.; Finkelshtein, A.L. X-ray Fluorescence Determination of Major Rock Forming Elements in Small Samples 50 and 110 Mg. *Anal. I Control.* **2015**, *19*, 130–138.
25. Perepelov, A.B.; Puzankov, M.Y.; Ivanov, A.V.; Filosofova, T.M.; Demonterova, E.I.; Smirnova, E.V.; Chuvashova, L.A.; Yasnygina, T.A. Neogene Basanites in Western Kamchatka: Mineralogy, Geochemistry, and Geodynamic Setting. *Petrology* **2007**, *15*, 488–508. [CrossRef]
26. Gurbanov, A.G.; Bogatikov, O.A.; Melekestsev, I.V.; Lipman, P.W.; Lowenstern, J.B.; Miller, D.R.; Dokuchaev, A.Y. The Elbrus Caldera in the Northern Caucasus: Geological Structure and Time of Formation. *Russ. J. Earth Sci.* **2004**, *6*, 251–255. [CrossRef]
27. Gazeev, V.M.; Nosova, A.A.; Sazonova, L.V.; Gurbanov, A.G.; Dokuchaev, A.Y. Petrogenetic Interpretation of Associations of Minerals-Distributors of Pleistocene-Holocene Volcanites of Elbrus (Northern Caucasus). *J. Volcanol. Seismol.* **2004**, *2*, 24–45.
28. Lebedev, V.A.; Chernyshev, I.V.; Chugaev, A.V.; Gol'tsman, Y.V.; Bairova, E.D. Geochronology of Eruptions and Parental Magma Sources of Elbrus Volcano, the Greater Caucasus: K-Ar and Sr-Nd-Pb Isotope Data. *Geochem. Int.* **2010**, *48*, 41–67. [CrossRef]
29. Regelous, A.; Scharfenberg, L.; De Wall, H. Origin of S-, A-and I-Type Granites: Petrogenetic Evidence from Whole Rock Th/U Ratio Variations. *Minerals* **2021**, *11*, 672. [CrossRef]

30. Churikova, T.; Dorendorf, F.; Wörner, G. Sources and Fluids in the Mantle Wedge below Kamchatka, Evidence from across-Arc Geochemical Variation. *J. Petrol.* **2001**, *42*, 1567–1593. [CrossRef]
31. Bindeman, I.N.; Wotzlaw, J.-F.; Stern, R.A.; Chiaradia, M.; Guillong, M.; Colón, D.P. Geochronology and Geochemistry Data for the Elbrus, Tyrnyauz, and Chegem Magmatic Centers, Greater Caucasus, Russia. *Data Brief* **2021**, *35*, 106896. [CrossRef] [PubMed]
32. Chernyshev, I.V.; Bubnov, S.N.; Lebedev, V.A.; Gol'tsman, Y.V.; Bairova, E.D.; Yakushev, A.I. Two Stages of Explosive Volcanism of the Elbrus Area: Geochronology, Petrochemical and Isotopic-Geochemical Characteristics of Volcanic Rocks, and Their Role in the Neogene-Quaternary Evolution of the Greater Caucasus. *Stratigr. Geol. Correl.* **2014**, *22*, 96–121. [CrossRef]
33. Sun, S.-S.; McDonough, W.F. Chemical and Isotopic Systematics of Oceanic Basalts: Implications for Mantle Composition and Processes. *Geol. Soc. Lond. Spec. Publ.* **1989**, *42*, 313–345. [CrossRef]
34. Rudnick, R.L.; Fountain, D.M. Nature and Composition of the Continental Crust: A Lower Crustal Perspective. *Rev. Geophys.* **1995**, *33*, 267–309. [CrossRef]
35. Hawkesworth, C.; Turner, S.; Peate, D.; McDermott, F.; Van Calsteren, P. Elemental U and Th Variations in Island Arc Rocks: Implications for U-Series Isotopes. *Chem. Geol.* **1997**, *139*, 207–221. [CrossRef]
36. Koulakov, I.; Zabelina, I.; Amanatashvili, I.; Meskhia, V. Nature of Orogenesis and Volcanism in the Caucasus Region Based on Results of Regional Tomography. *Solid Earth* **2012**, *3*, 327–337. [CrossRef]
37. Zabelina, I.; Koulakov, I.; Amanatashvili, I.; El Khrepy, S.; Al-Arifi, N. Seismic Structure of the Crust and Uppermost Mantle beneath Caucasus Based on Regional Earthquake Tomography. *J. Asian Earth Sci.* **2016**, *119*, 87–99. [CrossRef]
38. Lebedev, V.A.; Vashakidze, G.T. The Catalogue of Quaternary Volcanoes of the Greater Caucasus Based on Geochronological, Volcanological and Isotope-Geochemical Data. *J. Volcanol. Seismol.* **2014**, *8*, 93–107. [CrossRef]
39. Pearce, J.A.; Harris, N.B.; Tindle, A.G. Trace Element Discrimination Diagrams for the Tectonic Interpretation of Granitic Rocks. *J. Petrol.* **1984**, *25*, 956–983. [CrossRef]
40. Sisson, T.W.; Ratajeski, K.; Hankins, W.B.; Glazner, A.F. Voluminous Granitic Magmas from Common Basaltic Sources. *Contrib. Mineral. Petrol.* **2005**, *148*, 635–661. [CrossRef]
41. Müntener, O.; Kelemen, P.B.; Grove, T.L. The Role of H_2O during Crystallization of Primitive Arc Magmas under Uppermost Mantle Conditions and Genesis of Igneous Pyroxenites: An Experimental Study. *Contrib. Mineral. Petrol.* **2001**, *141*, 643–658. [CrossRef]
42. Annen, C.; Blundy, J.D.; Sparks, R.S.J. The Genesis of Intermediate and Silicic Magmas in Deep Crustal Hot Zones. *J. Petrol.* **2006**, *47*, 505–539. [CrossRef]
43. Melnik, O.E.; Utkin, I.; Bindeman, I.N. Magma Chamber Formation by Dike Accretion and Crustal Melting: 2D Thermo-Compositional Model with Emphasis on Eruptions and Implication for Zircon Records. *J. Geophys. Res.* **2021**, *126*, e2021JB023008. [CrossRef]
44. Williams, M.A.; Kelsey, D.E.; Baggs, T.; Hand, M.; Alessio, K.L. Thorium Distribution in the Crust: Outcrop and Grain-Scale Perspectives. *Lithos* **2018**, *320*, 222–235. [CrossRef]
45. Plank, T. Constraints from Thorium/Lanthanum on Sediment Recycling at Subduction Zones and the Evolution of the Continents. *J. Petrol.* **2005**, *46*, 921–944. [CrossRef]
46. Duggen, S.; Portnyagin, M.; Baker, J.; Ulfbeck, D.; Hoernle, K.; Garbe-Schönberg, D.; Grassineau, N. Drastic Shift in Lava Geochemistry in the Volcanic-Front to Rear-Arc Region of the Southern Kamchatkan Subduction Zone: Evidence for the Transition from Slab Surface Dehydration to Sediment Melting. *Geochim. Et Cosmochim. Acta* **2007**, *71*, 452–480. [CrossRef]
47. Yogodzinski, G.M.; Vervoort, J.D.; Brown, S.T.; Gerseny, M. Subduction Controls of Hf and Nd Isotopes in Lavas of the Aleutian Island Arc. *Earth Planet. Sci. Lett.* **2010**, *300*, 226–238. [CrossRef]
48. Liu, C.-Z.; Wu, F.-Y.; Chung, S.-L.; Li, Q.-L.; Sun, W.-D.; Ji, W.-Q. A 'Hidden'18 O-Enriched Reservoir in the Sub-Arc Mantle. *Sci. Rep.* **2014**, *4*, 4232. [CrossRef] [PubMed]
49. James, D.E. The Combined Use of Oxygen and Radiogenic Isotopes as Indicators of Crustal Contamination. *Annu. Rev. Earth Planet. Sci.* **1981**, *9*, 311–344. [CrossRef]
50. Kostitsyn, Y.A. Conditions of the Eldjurta Granite Formation According to Isotope Data (Oxygen and Strontium) in Vertical Profile. *Geokhimiya* **1995**, 780–797.
51. Ito, E.; White, W.M.; Göpel, C. The O, Sr, Nd and Pb Isotope Geochemistry of MORB. *Chem. Geol.* **1987**, *62*, 157–176. [CrossRef]
52. Nowell, G.M.; Kempton, P.D.; Noble, S.R.; Fitton, J.G.; Saunders, A.D.; Mahoney, J.J.; Taylor, R.N. High Precision Hf Isotope Measurements of MORB and OIB by Thermal Ionisation Mass Spectrometry: Insights into the Depleted Mantle. *Chem. Geol.* **1998**, *149*, 211–233. [CrossRef]
53. Savin, S.M.; Epstein, S. The Oyxgen and Hydrogen Isotope Geochemistry of Ocean Sediments and Shales. *Geochim. Et Cosmochim. Acta* **1970**, *34*, 43–63. [CrossRef]
54. Veizer, J.; Ala, D.; Azmy, K.; Bruckschen, P.; Buhl, D.; Bruhn, F.; Carden, G.A.; Diener, A.; Ebneth, S.; Godderis, Y. 87Sr/86Sr, Δ13C and Δ18O Evolution of Phanerozoic Seawater. *Chem. Geol.* **1999**, *161*, 59–88. [CrossRef]
55. Bucholz, C.E.; Jagoutz, O.; VanTongeren, J.A.; Setera, J.; Wang, Z. Oxygen Isotope Trajectories of Crystallizing Melts: Insights from Modeling and the Plutonic Record. *Geochim. Et Cosmochim. Acta* **2017**, *207*, 154–184. [CrossRef]
56. Bindeman, I. Oxygen Isotopes in Mantle and Crustal Magmas as Revealed by Single Crystal Analysis. *Rev. Mineral. Geochem.* **2008**, *69*, 445–478. [CrossRef]

57. Ishihara, S. The Magnetite-Series and Ilmenite-Series Granitic Rocks. *Min. Geol.* **1977**, *27*, 293–305.
58. Ishihara, S. The Redox State of Granitoids Relative to Tectonic Setting and Earth History: The Magnetite–Ilmenite Series 30 Years Later. *Earth Environ. Sci. Trans. R. Soc. Edinb.* **2004**, *95*, 23–33.
59. Clemente, B.; Scaillet, B.; Pichavant, M. The Solubility of Sulphur in Hydrous Rhyolitic Melts. *J. Petrol.* **2004**, *45*, 2171–2196. [CrossRef]
60. Babanskiy, A.D.; Ashikhmina, N.A.; Kovalenko, V.I. Parental magma for the rocks of the Upper Chegem Caldera (North Caucasus) from the results of studying inclusions in the minerals. *Dokl. Earth Sci.* **1995**, *344*, 226–228.
61. Tolstykh, M.L.; Naumov, V.B.; Gurbanov, A.G. The composition of Elbrus and Kazbek magmas from the study of inclusions in minerals. *Geokhimiya* **2001**, *4*, 441–448.
62. Loewen, M.W.; Bindeman, I.N.; Melnik, O.E. Eruption Mechanisms and Short Duration of Large Rhyolitic Lava Flows of Yellowstone. *Earth Planet. Sci. Lett.* **2017**, *458*, 80–91. [CrossRef]
63. Tuttle, O.F.; Bowen, N.L. *Origin of Granite in the Light of Experimental Studies in the System* $NaAlSi_3O_8$-$KAlSi_3O_8$-SiO_2-H_2O; Geological Society of America: Boulder, CO, USA, 1958; Volume 74.
64. Ebadi, A.; Johannes, W. Beginning of Melting and Composition of First Melts in the System Qz-Ab-Or-H_2O-CO_2. *Contrib. Mineral. Petrol.* **1991**, *106*, 286–295. [CrossRef]
65. Almeev, R.R.; Bolte, T.; Nash, B.P.; Holtz, F.; Erdmann, M.; Cathey, H.E. High-Temperature, Low-H2O Silicic Magmas of the Yellowstone Hotspot: An Experimental Study of Rhyolite from the Bruneau–Jarbidge Eruptive Center, Central Snake River Plain, USA. *J. Petrol.* **2012**, *53*, 1837–1866. [CrossRef]
66. Blundy, J.; Cashman, K. Ascent-Driven Crystallisation of Dacite Magmas at Mount St Helens, 1980–1986. *Contrib. Mineral. Petrol.* **2001**, *140*, 631–650. [CrossRef]